JOM, Vol. 71, No. 4, 2019
https://doi.org/10.1007/s11837-019-03333-x

Structures and Mechanical Properties of Al-Al_2Cu Interfaces

GUISEN LIU,[1] MINGYU GONG,[1] DONGYUE XIE,[1] and JIAN WANG[1,2]

1.—Mechanical and Materials Engineering, University of Nebraska-Lincoln, Lincoln, NE 68588, USA. 2.—e-mail: jianwang@unl.edu

Al-Cu eutectic composites are composed of α-Al and θ-Al_2Cu phases. Al-Al_2Cu interfaces play a crucial role in determining the deformation modes and mechanical properties of nanoscale Al-Cu composites. In this work, we studied the structures and properties of the $(110)_{Al_2Cu}\|(111)_{Al}$ interface and elucidated corresponding plastic deformation mechanisms by using atomistic simulations. The $(110)_{Al_2Cu}\|(111)_{Al}$ interface comprises three sets of Shockley partial dislocations that divide the interface into three types of coherent structures. The interface exhibits isotropic, low shear resistance corresponding to the easy gliding and threefold symmetry of interface dislocations. Under mechanical straining parallel to the interface, unusual slips occur on $\{011\}_{Al_2Cu}$ planes. Such an unexpected shear mode in Al_2Cu phase is ascribed to the slip continuity across the Al-Al_2Cu interface and the dislocations deposited at Al-Al_2Cu interfaces.

INTRODUCTION

Al-based eutectic composites, such as the Al-Si, Al-Ni, and Al-Cu systems, have been extensively studied because of their potential applications at ambient to elevated temperatures.[1–3] Al-Cu composites are composed of α-Al and θ-Al_2Cu phases. Depending on their composition ratio, α-Al and θ-Al_2Cu phases form alternating lamellae[4–7] or the θ-Al_2Cu phase may be present as precipitates in a matrix of α-Al.[8–10] α-Al with face-centered cubic (fcc) structure is ductile because of the available $\{111\}<110>$ slip systems. However, θ-Al_2Cu with C16 body-centered tetragonal (bct) structure[11] is brittle at room temperature due to high lattice friction stress for dislocation motion.[12,13] Experimental observations have confirmed a decrease in the brittle–ductile transition temperature (DBTT) of θ-Al_2Cu phase from 375°C in θ-Al_2Cu single crystals and polycrystals[14] to 300°C in microscale Al-Al_2Cu composites.[15] This lower DBTT in Al-Al_2Cu composites indicates that geometric constraints associated with interfaces may facilitate plastic deformation of ultrafine-scale θ-Al_2Cu phase.

The orientation relationships (ORs) and interface planes (IPs) of Al-Al_2Cu composites have been extensively characterized.[6,7,16,17] For Al-Al_2Cu eutectic with laminated microstructure, the most commonly observed OR is $\{211\}_{Al_2Cu}\|\{111\}_{Al}$ and $\langle 120\rangle_{Al_2Cu}\|\langle 110\rangle_{Al}$ when the layer thickness is greater than 1 μm. The interface plane is close to $\{211\}_{Al_2Cu}\|\{111\}_{Al}$.[16,17] For laser-remelted Al-Cu alloys where the layer thickness is in the range of tens to a few hundreds of nanometers, Al-Al_2Cu lamellar eutectic maintains the characteristic OR, $\{211\}_{Al_2Cu}\|\{111\}_{Al}$ and $\langle 120\rangle_{Al_2Cu}\|\langle 110\rangle_{Al}$, with two variants:[7,18,19] variant I retains $(001)_{Al_2Cu}\|\{001\}_{Al}$, while variant II has $(001)_{Al_2Cu}\|\{111\}_{Al}$ as interface planes. Al_2Cu precipitates are often formed in plate-like structures.[20,21] These precipitates develop several well-defined ORs with matrix α-Al,[22,23] viz. $(110)_{Al_2Cu}\|(111)_{Al}$ and $[1\bar{1}0]_{Al_2Cu}\|[1\bar{1}0]_{Al}$. The broad facets of Al_2Cu phase platelet particles are of $\{110\}_{Al_2Cu}$, which is parallel to $(111)_{Al}$ in matrix Al. This is due to the small lattice mismatch in the two orthogonal directions, with 1.23% mismatch in the $[1\bar{1}0]_{Al_2Cu}\|[1\bar{1}0]_{Al}$ and 1.71% mismatch in the $[001]_{Al_2Cu}\|[\bar{1}\bar{1}2]_{Al}$.

Interfaces have been demonstrated to play a significant role in determining the plastic deformation modes and mechanical properties of heterogeneous composites.[24–28] Interfaces can act as barriers for impeding dislocations, thereby strengthening materials. In particular, the weak shear interface

(Published online January 14, 2019)

has a stronger blocking effect on lattice dislocations due to core spreading of dislocations on the weak interface, as demonstrated by Cu-Nb interfaces.[24,29,30] Interfaces with high diffusivity and low energy of formation for point defects can act as sinks for recovery and/or reassembly of defects to reduce stress concentrations, leading to high plastic flow stability.[31–33] On the other hand, interfaces can act as sources for nucleating interfacial dislocations[24,29] and lattice dislocations,[30,34–36] facilitating interface shear and slip transmission or transmutation. Thus, knowledge regarding the structures and properties of Al-Al_2Cu interfaces is essential to understand the role of interfaces in determining the mechanical properties of Al-Cu composites.

The atomic structures of interfaces associated with the two ORs in Al-Cu eutectic laminates were characterized recently using microscopes[6] and modeled using atomistic simulations.[7] In the work presented herein, we studied the structures and properties of the $(110)_{Al_2Cu}\|(111)_{Al}$ interface and elucidated corresponding plastic deformation mechanisms of nanoscale Al-Al_2Cu laminates by using molecular dynamics/statics (MD/MS) simulations.

Molecular Dynamics Simulations

Using atomistic simulations with empirical potentials, we studied the structures and mechanical properties of the $(110)_{Al_2Cu}\|(111)_{Al}$ interface. The potentials have been tested to well reproduce lattice constants, cohesive energy, and elastic properties, in comparison with density functional theory calculations and experiments,[37,38] and the core structure and mobility of dislocations associated with possible slip systems in θ-Al_2Cu.[12,39] The essential details of the atomistic simulations are described below.

The study of interface structure and interface shear adopts a bicrystal structure. The bicrystal model of Al and Al_2Cu is created and assembled from two unrelaxed semiinfinite perfect crystals with ORs of $(110)_{Al_2Cu}\|(111)_{Al}$, $[1\bar{1}0]_{Al_2Cu}\|[1\bar{1}0]_{Al}$, and $[001]_{Al_2Cu}\|[\bar{1}\bar{1}2]_{Al}$. Due to the lattice mismatch, we choose the specific dimension of 18.63 nm in the $[1\bar{1}0]_{Al_2Cu}\|[1\bar{1}0]_{Al}$ direction (the x-direction), corresponding to 65 units for Al and 22 units for Al_2Cu, and 31.27 nm in the $[001]_{Al_2Cu}\|[\bar{1}\bar{1}2]_{Al}$ direction (the z-direction), corresponding to 63 units for Al and 64 units for Al_2Cu, to ensure minimum internal strain in the bicrystal model. The interface plane is in the x–z plane. Periodic boundary conditions are applied for the x and z directions. The dimension for the $[110]_{Al_2Cu}\|[111]_{Al}$ direction (the y-direction) is 50 nm for each. The semirigid regions act as a fixed boundary during relaxation. The thickness of semirigid region in the y-direction is 1 nm for the two crystals. Relaxation of the bicrystal model is accomplished by the quenching molecular dynamics method. During relaxation, the two crystals can translate in three directions, but rotation is not allowed. Interface structures are obtained when the maximum force acting on atoms is less than 5 pN. Coherent interfaces and misfit dislocations are analyzed and characterized by disregistry analysis[29] and atomistically informed Frank–Bilby theory.[40]

The shear resistance of the interface is investigated by applying a gradually increasing shear strain homogeneously to the relaxed bicrystal. The shear stresses τ_{yx} and τ_{yz} on the interface are generated by applying the displacement gradients, $\frac{\partial u}{\partial y}$ and $\frac{\partial w}{\partial y}$, to the two crystals. u and w are the displacements along x and z direction. Shearing of the two crystals is achieved in the two crystals while maintaining equilibrium at each loading step. After applying the displacement gradient increments to the two crystals, all atomic positions are allowed to relax fully and independently.[29]

To explore the role of the interface in triggering plastic deformation events in Al_2Cu phase, we construct a sandwich structure composed of a middle layer of 3-nm-thick Al_2Cu and two 4-nm-thick Al layers. Periodic boundary conditions are applied in the x- and z-directions and free surfaces in the y-direction. We conduct uniaxial stress tensile testing along $[001]_{Al_2Cu}$ direction with a strain increment of 0.2% per 10 ps using MD simulations. A finite temperature of 10 K is maintained during straining.

RESULTS AND DISCUSSION

Structures and Energies of $(110)_{Al_2Cu}\|(111)_{Al}$ Coherent Interfaces

Corresponding to the crystallography of the OR and IP associated with the bicrystal, there are four possible interfaces with respect to the termination of Al_2Cu phase. Figure 1a shows the unit structure of Al_2Cu phase. The terminated plane of Al_2Cu phase can be Cu, one Al layer, two Al layers, or three Al layers. Figure 1b shows the projection of the unit structure on the $[110]_{Al_2Cu}$ direction. Note that these atomic planes can form hexagonal patterns even though each plane contains different numbers of atoms: four Cu atoms in one Cu plane, four Al atoms in one Al_B or Al_D plane, and two Al atoms in one Al_A or Al_C plane. Note also that the translation between Al_A and Al_C or between Al_B and Al_D can be achieved through in-plane shear of $\frac{1}{2}<001>_{Al_2Cu}$. If we refer to the terminated plane of Al_2Cu layer as A plane with respect to the …ABCABC… stacking sequence according to the stacking sequence of (111) planes in an fcc structure, the first atomic plane of Al layer can take the position of a B plane, forming a normal fcc stacking structure. Atomistic simulations reveal that two interfaces are stable, associated with a terminated plane of two (Fig. 1d) or three Al layers (Fig. 1f). In the case of the Cu-terminated interface, the first

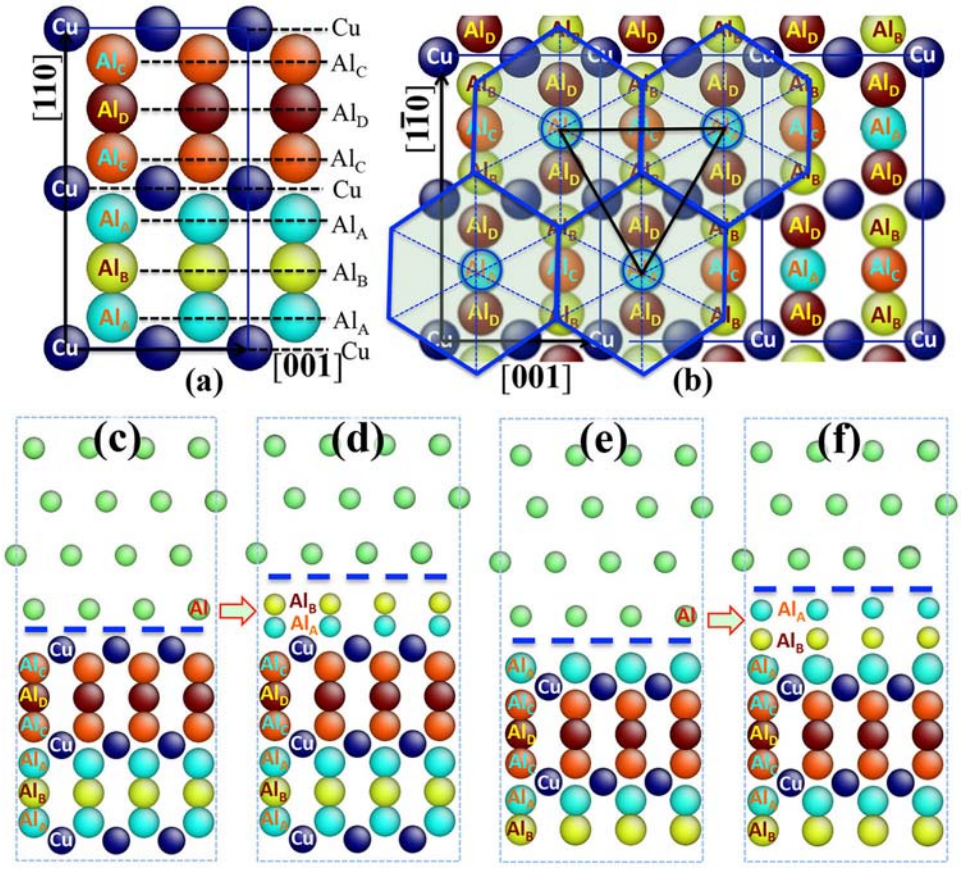

Fig. 1. Atomic structures of projection of unit cell of Al_2Cu along (a) [1$\bar{1}$0] and (b) [110]. One periodic (110) plane contains eight atomic planes with stacking sequence …$CuAl_AAl_BAl_ACuAl_CAl_DAl_C$…. The relative position of atoms in the stack is shown in (b). Blue rectangles outline the unit cell on the projected plane. Atoms in each plane can form a hexagonal pattern. Atomic structures of Al-Al_2Cu interfaces, showing that (c, d) the first Al plane in Al layer decomposes into two Al planes Al_AAl_B in the Cu-terminated case, and (e, f) the first Al plane in Al layer decomposes into two Al planes Al_BAl_A in the one Al-layer terminated case.

$(111)_{Al}$ plane in Al phase will decompose into two Al layers of Al_2Cu phase (Fig. 1c and d). The resulting interface is the same as the terminated interface with two Al layers. In the case of the terminated interface with one Al layer, the first $(111)_{Al}$ plane in Al phase will decompose into two Al layers of Al_2Cu phase (Fig. 1e and f). The resulting interface is the same as the terminated interface with three Al layers.

Relaxed, equilibrium semicoherent interfaces are generally composed of interface dislocations and coherent interface patches. Structures and energies of formation of coherent interfaces will determine the equilibrium interface structure and interface dislocations. Here, we first study the structures and energy of formation of coherent interfaces. Corresponding to an fcc structure, there are three typical coherent structures: high-energy stacking fault (HESF) structure, normal fcc structure, and intrinsic stacking fault (SF) structure (Fig. 2a, b, and c). Figure 2d shows the generalized stacking fault energy (GSFE) surface associated with the terminated interface with two layers of Al. The fcc and SF structures correspond to energy minima on the GSFE surface of 740 mJ/m^2 and 790 mJ/m^2, respectively, meaning that they are stable. The HESF is a metastable interface with energy of formation of 1040 mJ/m^2. Compared with the terminated interface with two Al layers, that with three Al layers has high energy of formation of about 1470 mJ/m^2. The discussion and simulations presented below focus on the terminated interface with two Al layers.

Dislocations of $(110)_{Al_2Cu}\|(111)_{Al}$ Semicoherent Interface

Figure 3a shows the atomic structure of the unrelaxed Al/Al_2Cu interface. Using a geometry analysis approach according to the (111) plane stacking with respect to an fcc structure, the unrelaxed interface can be classified into four regions, viz. near-FCC [normal (111) stacking], near-SF (the intrinsic stacking fault), the region separating the FCC from SF regions (referred to as the dislocation region, occupied by unstable stacking fault), and the HESF region around the coincident site (or around the node which has high-energy stacking fault structure). After relaxation at zero temperature using the dynamic-quenching MD

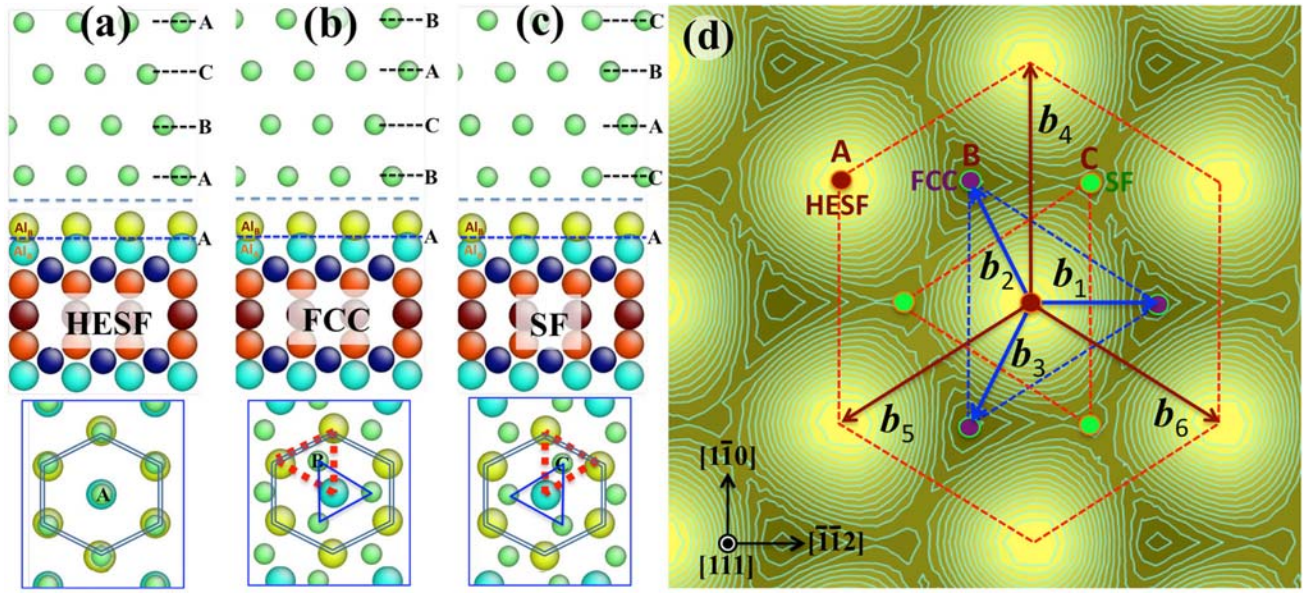

Fig. 2. Atomic structures of coherent interfaces: (a) high-energy stacking fault (HESF) structure, (b) normal fcc structure, and (c) intrinsic stacking fault (SF) structure. (d) The generalized stacking fault energy (GSFE) surface associated with the terminated interface with two layers of Al. Three partial dislocations with Burgers vectors $\boldsymbol{b}_1$, $\boldsymbol{b}_2$, and $\boldsymbol{b}_3$ and three full dislocations with Burgers vectors of $\boldsymbol{b}_4$, $\boldsymbol{b}_5$, and $\boldsymbol{b}_6$ are illustrated in (d).

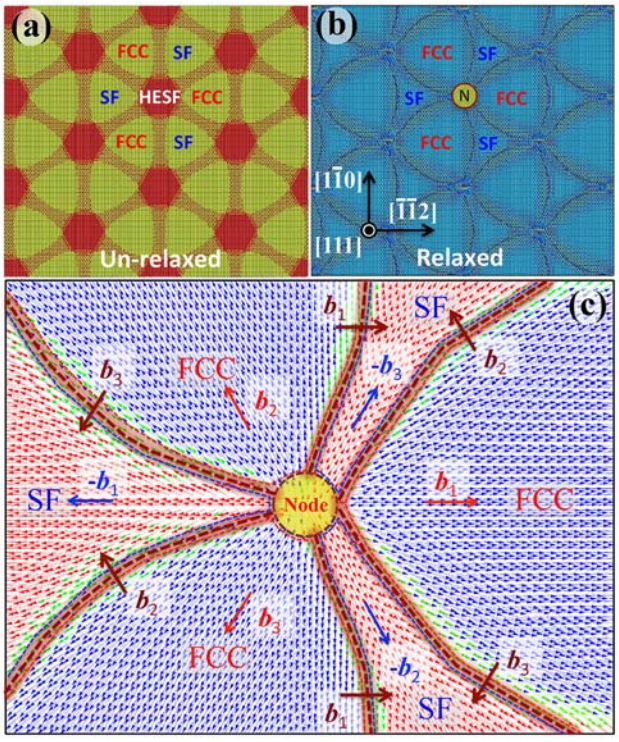

Fig. 3. Atomic structures of (a) unrelaxed interface and (b) relaxed interface at zero temperature, showing the dislocations and coherent interface patterns. Atoms are colored by the number of neighbors. (c) Disregistry plots of the interface around a node, showing characters of interface dislocations and the relaxation mechanisms through expansion or shrinkage of Shockley partial dislocation loops.

method, the relaxed interface (Fig. 3b) exhibits a repeatable pattern comprising six coherent regions around one node. Three sets of interface dislocations intersect to form the node and divide the region into six coherent patches. Figure 3c shows the disregistry plots of the interface before and after relaxation. The near-FCC and near-SF regions are enclosed by an array of Shockley partial dislocation loops with respect to a coherent (111) interface. These dislocations have Burgers vectors, $\boldsymbol{b}_1$, $-\boldsymbol{b}_3$, $\boldsymbol{b}_2$, $-\boldsymbol{b}_1$, $\boldsymbol{b}_3$, and $-\boldsymbol{b}_2$. $\boldsymbol{b}_1 = \frac{a}{6}[\bar{1}\bar{1}2]$, $\boldsymbol{b}_2 = \frac{a}{6}[2\bar{1}\bar{1}]$, and $\boldsymbol{b}_3 = \frac{a}{6}[\bar{1}2\bar{1}]$ are defined in Fig. 2d. Upon energy minimization, the reduction in chemical potential energy (coherency) drives the near-FCC and near-SF regions to become FCC and SF regions, accompanying the expansion or shrinkage of Shockley partial dislocation loops. The six partial loops react and form six segmental dislocations around a node. The bold dashed lines indicate the dislocations, and the shadow regions outline the core width of the dislocation.

HESF region relaxes through local rotation and local in-plane dilatation or shrinkage of the two crystals at a node.[41] According to crystallography, the relative rotation across the interface plane can destroy the HESF structure, leading to three near-FCC structures and three near-intrinsic stacking fault (ISF) structures around the node. When the quenched structure is further relaxed at a temperature of 10 K, the HESF region rotates and shifts, destroying the HESF structure and forming a SF structure between the first and second (111) planes in Al. An intrinsic stacking faulted triangle forms in Al, as shown in Fig. 4b. The Al-Al_2Cu interface is shown in Fig. 4c. The stacking sequence around the node is illustrated in Fig. 4e. As a result, misfit dislocations form in the interface between Al and Al_2Cu and in the interface between the first and

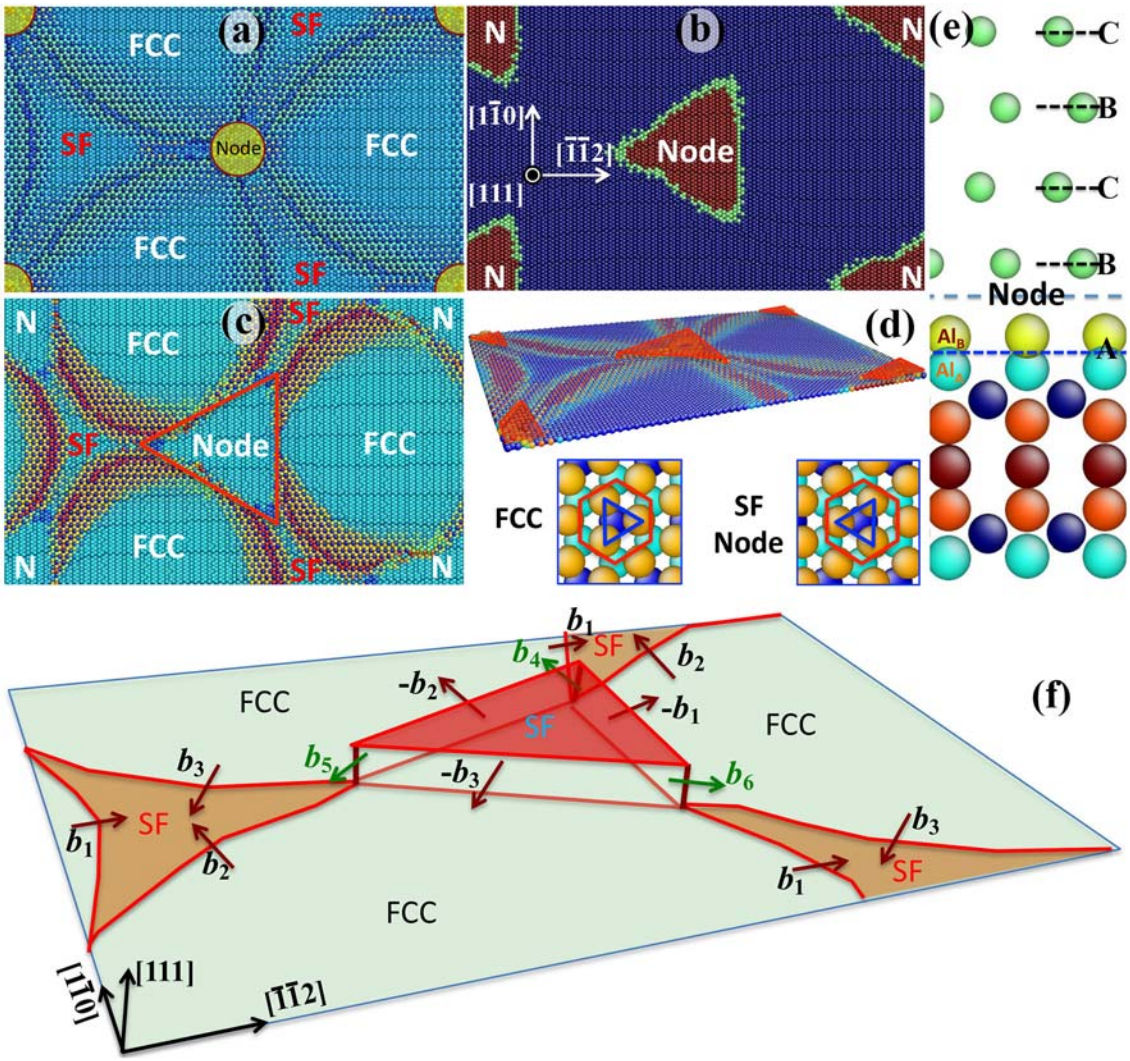

Fig. 4. (a) Atomic structure of zero-temperature relaxed interface. (b) Atomic structures of relaxed interface at 10 K, showing an intrinsic stacking faulted triangle between the first and second (111) planes in Al and (c) the interface between Al and Al_2Cu. The formation of faulted structure is associated with the evolution of the node structure. Atoms are colored by the numbers of neighbors in (a) and (c) and the common neighboring analysis in (b). (d, e) Illustration of node structures and (f) patterns and characters of interface dislocations.

second (111) planes in Al, as shown in Fig. 4d and e. $b_4 = \frac{a}{2}[1\bar{1}0]$, $b_5 = \frac{a}{2}[01\bar{1}]$, and $b_6 = \frac{a}{2}[\bar{1}01]$ are mobile jogs with length of one atomic plane thickness. The corresponding relaxation mechanisms and characteristic dislocations observed in the Al-Al_2Cu interface are similar to those occurring in (111) semicoherent fcc interfaces.[42]

Mechanical Properties of $(110)_{Al_2Cu}\|(111)_{Al}$ Interface

Figure 5 shows the shear stress–strain curve and shear response of the $(110)_{Al_2Cu}\|(111)_{Al}$ semicoherent interface when the bicrystal model is subjected to shear stress along the $[\bar{1}10]_{Al_2Cu}$ direction. The result shows low shear resistance of 200 MPa in Fig. 5a. More interestingly, slip occurs only on the Al-Al_2Cu interface. Figure 5b, d, and f shows the evolution of the dislocation structure in the Al-Al_2Cu interface, while Fig. 5c, e, and g shows the evolution of the dislocation structure in the interface between the first and second (111) planes in Al at shear strain of 0.0, 0.015, and 0.025, respectively. Note that the interface dislocation pattern remains, with only slight changes in the shape of dislocation lines, implying that interface slip is achieved through glide of interface dislocations. The low shear resistance is attributed to easy glide of interface dislocations. When the bicrystal model is sheared along different in-plane directions, we observe the same shear resistance and the same shear mechanism, which is ascribed to the threefold symmetry of the interface structure and interface dislocations on the Al-Al_2Cu interface.

When the sandwich structure (Fig. 6a) is subjected to uniaxial tensile stress along the $[001]_{Al_2Cu}$

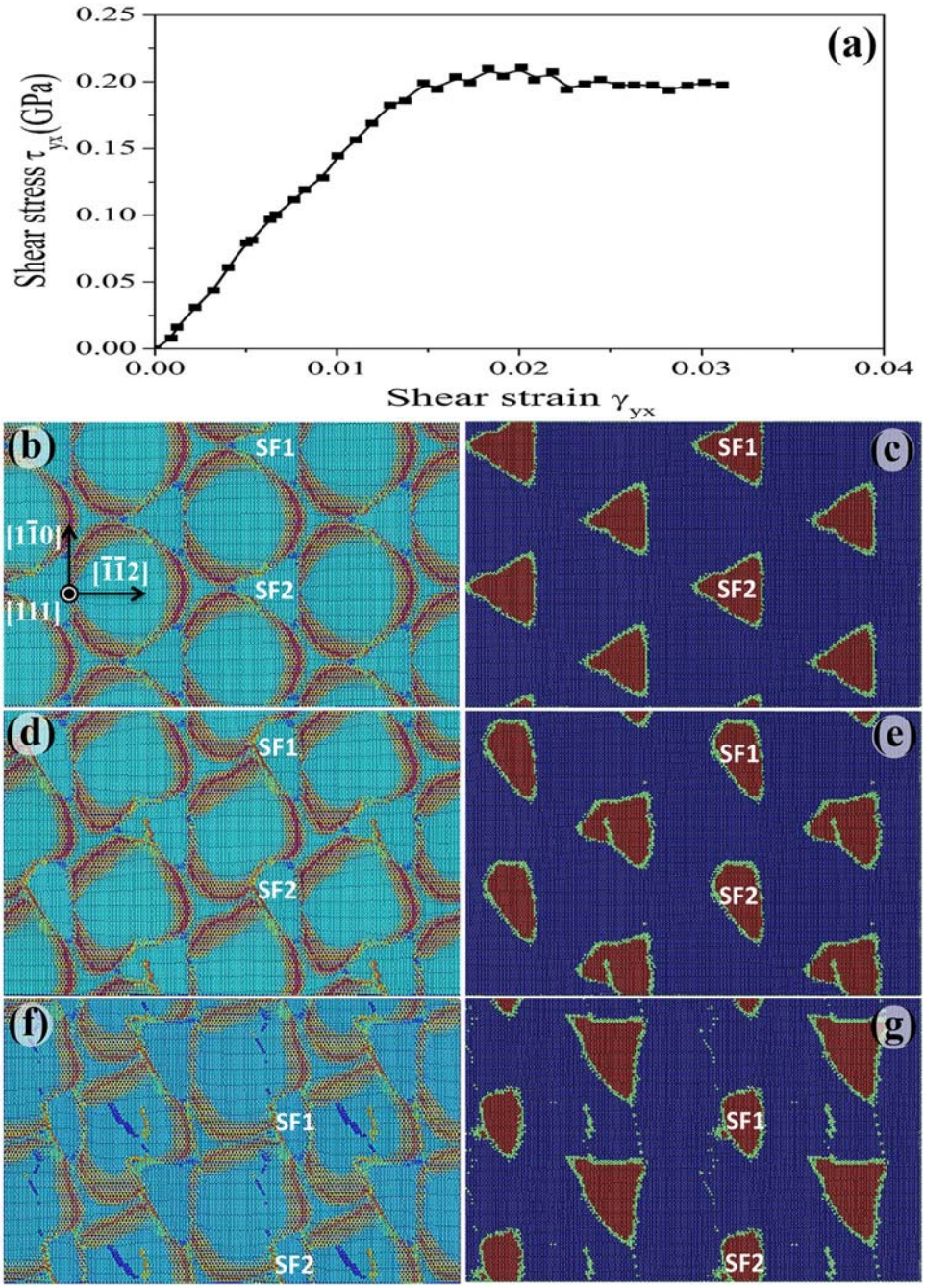

Fig. 5. Shear response of the Al-Al_2Cu interface. (a) The shear stress–strain curve as the bicrystal is sheared along $[\bar{1}10]_\theta$. The evolution of interface dislocations in the Al-Al_2Cu interface (b, d, f) and the interface between the first and second (111) planes in Al (c, e, g) at shear strain of 0.0, 0.015, and 0.025, respectively. Atoms are colored by the numbers of neighbors in (b, d, f) and the common neighboring analysis in (c, e, g).

direction, Fig. 6b plots the stress–strain response, showing an obvious nonlinear response commencing at tensile strain of 0.022, which corresponds to tensile stress of 2.3 GPa. With continuing tension, plastic deformation develops in Al layers and then in both Al and Al_2Cu layers. Figure 6c and d show the atomic structures of the deformed structure at tensile strain of 0.03 and 0.09, respectively. Note that steps along $<110>_{Al}$ form on the two free surfaces of the two Al layers, and the numbers and height of $<110>_{Al}$ steps increase with the tensile strain. These steps are slip traces, as dislocations associated with $\{111\}<110>$ slip systems glide out of the Al layers. The interaction of dislocations in Al layers results in strain hardening, as observed in Fig. 6b. When the tensile strain exceeds 0.08, the Al_2Cu layer deforms plastically. Figure 6e, f shows atomic structures of the Al_2Cu layer, revealing slip

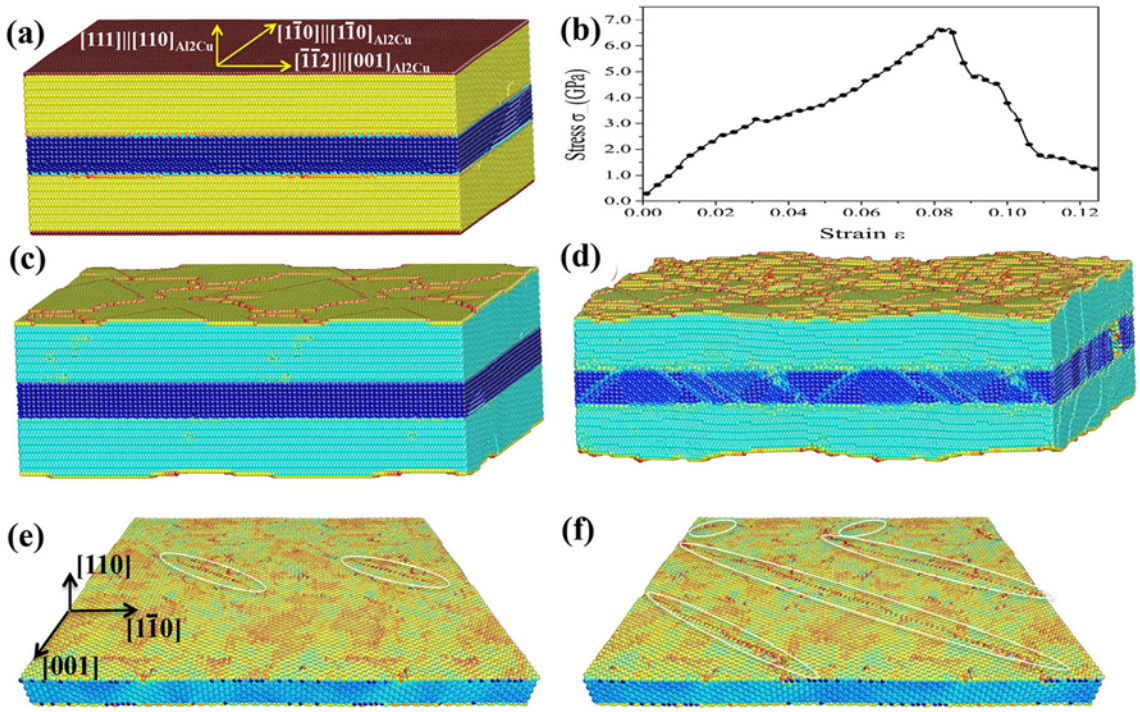

Fig. 6. (a) Sandwich structure of Al/Al_2Cu/Al laminate. (b) Stress–strain response associated with uniaxial stress tension along $[001]_{Al_2Cu}$ direction. (c, d) Atomic structures of deformed structure at tensile strain of 0.03 and 0.09, showing steps along $<110>_{Al}$ on the two free surfaces of the two Al layers and shears in Al_2Cu. (e, f) Atomic structures of Al_2Cu layer, revealing slip traces parallel to $<111>_{Al_2Cu}$. Atoms colored by the number of neighbors.

traces parallel to $<111>_{Al_2Cu}$. According to crystallography of Al_2Cu phase, we identified the slip planes to be $\{011\}_{Al_2Cu}$ planes.

It is worth mentioning that $\{011\}_{Al_2Cu}$ planes are not a well-recognized slip plane in θ-Al_2Cu. Experimental observations and theoretical calculations based on crystal structure revealed slip planes {110}, {100}, {011}, and {112} in θ-Al_2Cu phase.[7,12,15,43] Our previous molecular dynamics simulations revealed that only edge dislocations associated with (110)<001>, (010)<001>, and (310)<001> slip systems could glide at room temperature.[12] Thus, shearing on $\{011\}_{Al_2Cu}$ plane might be triggered by slip transmission across interfaces. The transmissibility of slip across an interface depends on the applied stress, internal stress, energy barriers associated with the transmission of a dislocation across the interface, and the geometric alignment of slip systems (slip planes and vectors) across the interface.[30,44] Our first-principles density functional theory calculations suggested that shearing of $\{011\}_{Al_2Cu}$ plane must be achieved under high shear stress.[12] In our MD simulations, high shear stress on $(0\bar{1}1)$ plane is contributed by both applied tensile stress and internal stress associated with the attractive force due to dislocations deposited at the interfaces. Figure 7a shows the nucleation and emission of dislocations associated with slip systems {111}<110> in Al layers. Interface dislocations act as sources for nucleating these dislocations. These dislocations propagate in Al layers and deposit at the two Al-Al_2Cu interfaces. For a sandwich structure, these deposited dislocations associated with the same slip system at the two interfaces have the opposite line sense but the same Burgers vector, resulting in a strong attractive force on each other.[45] In addition, these deposited dislocations generate maximum shear stress on planes in Al_2Cu layer which are parallel to {111} planes in Al layers.[46] Using crystallographic analysis, Fig. 7b shows the geometrical relationship between {011} planes in Al_2Cu layer and {111} planes in Al layer. Note that two pairs of {111}-{011} slip planes are nearly parallel. Moreover, the slip traces associated with the two pairs of slip planes on the interface are nearly parallel with a small deviation angle of 0.03°. Corresponding to the slip continuity across the interface based on crystallographic analysis, highly localized shear stress will develop on {011} planes in Al_2Cu layer and increases with the density of deposited dislocations. The unexpected plasticity mechanism of shearing on $\{011\}_{Al_2Cu}$ planes is ascribed to the slip continuity across the interface between Al and Al_2Cu layers and localized shear stress on $\{011\}_{Al_2Cu}$ planes due to the interaction of and shear stress field associated with deposited dislocations. Interestingly, our recent experimental study confirmed such shears on $\{011\}_{Al_2Cu}$ planes in laser-processed nanoscale Al-Al_2Cu eutectic alloy.[7]

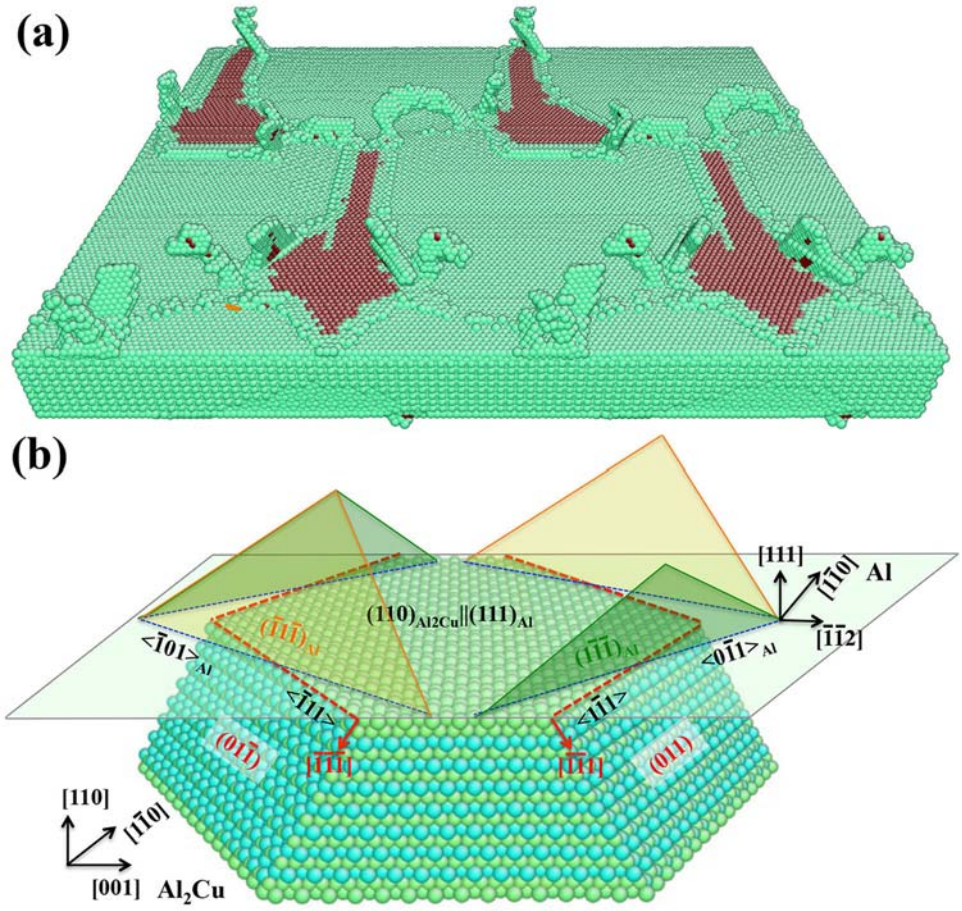

Fig. 7. (a) Atomic structure of the sandwich structure at tensile strain of 0.02, showing dislocation loops in Al layer that nucleate from interface dislocations. The regions comprising red atoms are the stacking fault structure in the second (111) plane in Al layer. (b) Schematic of the geometrical relationship between {011} planes in Al_2Cu layer and {111} planes in Al layer.

CONCLUSION

Using atomistic simulations, we studied the structures and mechanical properties of the $(110)_{Al_2Cu}\|(111)_{Al}$ interface and elucidated corresponding plastic deformation mechanisms. The atomistic simulations revealed two stable interfaces, associated with a terminated interface of two or three Al layers. The former has lower energy of formation than the latter. For the low-energy interface, the $(110)_{Al_2Cu}\|(111)_{Al}$ interface comprises three sets of Shockley partials that divide the interface into three types of coherent interface. The interface exhibits isotropic, low shear resistance, which is ascribed to the easy gliding and threefold symmetry of interface dislocations on the interface. Under mechanical straining parallel to the interface, unusual slips occur on {110} planes in Al_2Cu phase. Such a new deformation mode in Al_2Cu phase is ascribed to the slip continuity across the Al-Al_2Cu interface and the dislocations deposited at Al-Al_2Cu interfaces.

ACKNOWLEDGEMENTS

This research is sponsored by the DOE, Office of Science, Office of Basic Energy Sciences under award no. DE-SC0016808. The authors also thank Dr. Qing Zhou and Ms. Lin Chen for valuable discussion while visiting UNL. Atomistic simulations were conducted at the Holland Computing Center (HCC), a high-performance computing resource for the University of Nebraska System.

REFERENCES

1. J.M. Park, N. Mattern, U. Kühn, J. Eckert, K.B. Kim, W.T. Kim, K. Chattopadhyay, and D.H. Kim, *J. Mater. Res.* 24, 2605 (2009).
2. J. Park, K. Kim, D. Kim, N. Mattern, R. Li, G. Liu, and J. Eckert, *Intermetallics* 18, 1829 (2010).
3. X.P. Li, X.J. Wang, M. Saunders, A. Suvorova, L.C. Zhang, Y.J. Liu, M.H. Fang, Z.H. Huang, and T.B. Sercombe, *Acta Mater.* 95, 74 (2015).
4. M. Zimmermann, M. Carrard, and W. Kurz, *Acta Metall.* 37, 3305 (1989).
5. X. Li, Z. Ren, Y. Fautrelle, Y. Zhang, and C. Esling, *Acta Mater.* 58, 1403 (2010).
6. S.J. Wang, G. Liu, J. Wang, and A. Misra, *Mater. Charact.* 142, 170 (2018).

7. S.J. Wang, G. Liu, D.Y. Xie, Q. Lei, B.P. Ramakrishnan, J. Mazumder, J. Wang, and A. Misra, *Acta Mater.* 156, 52 (2018).
8. M. Aravind, P. Yu, M.Y. Yau, and D.H.L. Ng, *Mater. Sci. Eng., A* 380, 384 (2004).
9. E.F. Prados, V.L. Sordi, and M. Ferrante, *Acta Mater.* 61, 115 (2013).
10. A.A. Csontos and E.A. Starke, *Int. J. Plast* 21, 1097 (2005).
11. A. Meetsma, J.L. De Boer, and S. Van Smaalen, *J. Solid State Chem.* 83, 370 (1989).
12. Q. Zhou, J. Wang, A. Misra, P. Huang, F. Wang, and K. Xu, *Int. J. Plast.* 87, 100 (2016).
13. A. Yanilkin, V. Krasnikov, A.Y. Kuksin, and A. Mayer, *Int. J. Plast.* 55, 94 (2014).
14. T. Chanda and G.S. Murty, *J. Mater. Sci.* 27, 5931 (1992).
15. M. Ignat, R. Bonnet, D. Caillard, and J.L. Martin, *Phys. Status Solidi A* 49, 675 (1978).
16. G. Davies and A. Hellawell, *Philos. Mag.: J. Theor. Exp. Appl. Phys.* 22, 1255 (1970).
17. W. Zhu, Z. Ren, W. Ren, Y. Zhong, and K. Deng, *Mater. Sci. Eng., A* 441, 181 (2006).
18. B. Cantor and G.A. Chadwick, *J. Cryst. Growth* 23, 12 (1974).
19. V.T. Witusiewicz, U. Hecht, S. Rex, and J. Cryst, *Growth* 372, 57 (2013).
20. K.G. Russell and M. Ashby, *Acta Metall.* 18, 891 (1970).
21. R. Bonnet and M. Loubradou, *Phys. Status Solidi A* 194, 173 (2002).
22. C. Hadj Belgacem, M. Fnaiech, M. Loubradou, S. Lay, and R. Bonnet, *Phys. Status Solidi A* 189, 183 (2002).
23. K. Gao, S. Li, L. Xu, and H. Fu, *J. Cryst. Growth* 394, 89 (2014).
24. J. Wang and A. Misra, *Curr. Opin. Solid St. Mater. Sci.* 15, 20 (2011).
25. I.J. Beyerlein, M.J. Demkowicz, A. Misra, and B.P. Uberuaga, *Prog. Mater Sci.* 74, 125 (2015).
26. X. Ma, C. Huang, J. Moering, M. Ruppert, H.W. Höppel, M. Göken, J. Narayan, and Y. Zhu, *Acta Mater.* 116, 43 (2016).
27. T. Shimokawa, T. Oguro, M. Tanaka, K. Higashida, and T. Ohashi, *Mater. Sci. Eng., A* 598, 68 (2014).
28. J. Wang, Q. Zhou, S. Shao, and A. Misra, *Mater. Res. Lett.* 5, 1 (2017).
29. J. Wang, R.G. Hoagland, J.P. Hirth, and A. Misra, *Acta Mater.* 56, 3109 (2008).
30. J. Wang, A. Misra, R. Hoagland, and J. Hirth, *Acta Mater.* 60, 1503 (2012).
31. X. Zhang, K. Hattar, Y. Chen, L. Shao, J. Li, C. Sun, K. Yu, N. Li, M.L. Taheri, H. Wang, J. Wang, and M. Nastasi, *Prog. Mater Sci.* 96, 217 (2018).
32. A.S. Budiman, K.R. Narayanan, N. Li, J. Wang, N. Tamura, M. Kunz, and A. Misra, *Mater. Sci. Eng., A* 635, 6 (2015).
33. N. Li, J. Wang, J.Y. Huang, A. Misra, and X. Zhang, *Scripta Mater.* 63, 363 (2010).
34. R.F. Zhang, J. Wang, I.J. Beyerlein, A. Misra, and T.C. Germann, *Acta Mater.* 60, 2855 (2012).
35. S. Shao, J. Wang, I.J. Beyerlein, and A. Misra, *Acta Mater.* 98, 206 (2015).
36. I.J. Beyerlein, J. Wang, and R. Zhang, *Acta Mater.* 61, 7488 (2013).
37. F. Apostol and Y. Mishin, *Phys. Rev. B* 83, 054116 (2011).
38. N. Fribourg-Blanc, M. Dupeux, G. Guenin, and R. Bonnet, *J. Appl. Crystallogr.* 12, 151 (1979).
39. Q. Zhou, J. Wang, A. Misra, P. Huang, F. Wang, and K. Xu, *NPJ Comput. Mater.* 3, 24 (2017).
40. J. Wang, R. Zhang, C. Zhou, I.J. Beyerlein, and A. Misra, *J. Mater. Res.* 28, 1646 (2013).
41. S. Shao, J. Wang, and A. Misra, *J. Appl. Phys.* 116, 023508 (2014).
42. S. Shao, J. Wang, A. Misra, and R.G. Hoagland, *Sci. Rep.* 3, 2448 (2013).
43. M. Ignat and F. Durand, *Scripta Metall.* 10, 623 (1976).
44. W. Clark, R. Wagoner, Z. Shen, T. Lee, I. Robertson, and H. Birnbaum, *Scripta Metall. Mater.* 26, 203 (1992).
45. J. Wang and A. Misra, *Curr. Opin. Solid State Mater. Sci.* 18, 19 (2014).
46. J.P. Hirth and J. Lothe, *Theory of Dislocations*, 2nd ed. (Hoboken: Wiley, 1982).